



Article

Laser Processing of Ni-Based Superalloy Surfaces Susceptible to Stress Concentration

Boris Rajčić ^{1,*} , Sanja Petronić ², Katarina Čolić ³, Zoran Stević ⁴, Ana Petrović ⁵, Žarko Mišković ⁵ 
and Dubravka Milovanović ¹

¹ Institute of General and Physical Chemistry, 11000 Belgrade, Serbia; dubravka.milovanovic2007@gmail.com

² Department of Belgrade Polytechnic, The Academy of Applied Technical Studies Belgrade, 11000 Belgrade, Serbia; spetronic@politehnika.edu.rs

³ Innovation Centre of the Faculty of Mechanical Engineering, 11000 Belgrade, Serbia; kbojic@mas.bg.ac.rs

⁴ Technical Faculty, Bor, School of Electrical Engineering, University of Belgrade, 11000 Belgrade, Serbia; zstevic@etf.rs

⁵ Faculty of Mechanical Engineering, University of Belgrade, 11000 Belgrade, Serbia; aspetrovic@mas.bg.ac.rs (A.P.); zmiskovic@mas.bg.ac.rs (Ž.M.)

* Correspondence: borisrajcic@gmail.com; Tel.: +381-64-117-62-65

Abstract: Reliable and resilient constructions are basic for ensuring the safety of various structures. The superalloys are used as constructive materials due to their superb mechanical properties and endurance. However, even these materials can have certain areas where the stress concentration is higher than expected, such as drilling holes, which are common in various structures that need additional enhancement. Surface laser modifications of the areas surrounding the holes drilled in Nimonic 263 sheets are done by pulsed picosecond and nanosecond Nd:YAG laser irradiations with pulse durations of 170 ps and ≤ 8 ns, respectively. Following the laser surface treatment, the effectiveness of the enhancement was analyzed by the microhardness test and the deformation test. The results show that the deformation and stress values are decreased by 25–40 percent, showing the improvement in the resilience to deformation. The Vickers microhardness test results indicate an improvement in the Nimonic 263 microhardness. The dimensions of the microcracks are higher for the untreated material in comparison to the laser-treated material.

Keywords: Nimonic 263 alloy; surface modification; laser processing; digital image correlation (DIC) method



Citation: Rajčić, B.; Petronić, S.; Čolić, K.; Stević, Z.; Petrović, A.; Mišković, Ž.; Milovanović, D. Laser Processing of Ni-Based Superalloy Surfaces Susceptible to Stress Concentration. *Metals* **2021**, *11*, 750. <https://doi.org/10.3390/met11050750>

Academic Editors: Thomas Niendorf and Koji Kakehi

Received: 31 March 2021

Accepted: 28 April 2021

Published: 1 May 2021

Publisher's Note: MDPI stays neutral with regard to jurisdictional claims in published maps and institutional affiliations.



Copyright: © 2021 by the authors. Licensee MDPI, Basel, Switzerland. This article is an open access article distributed under the terms and conditions of the Creative Commons Attribution (CC BY) license (<https://creativecommons.org/licenses/by/4.0/>).

1. Introduction

Excellent mechanical properties (high modulus of elasticity, hardness, toughness and wear resistance), structure stability and high corrosion resistance under high temperatures, make the nickel-based superalloys a suitable candidate for a wide range of applications, such as in aircraft technology, the gas and oil industry, and other facilities with extreme working conditions [1–6].

The nickel-based superalloy studied in this work is the Nimonic 263, a centered cubic austenite crystal structure alloy with superb surface stability, high corrosion and oxidation resistance, thanks to the aluminum and chromium present in the alloy, high mechanical strength, excellent flexible properties, which makes it convenient for both hot and cold working processes, as well as good weldability and formability, compared to other nickel-based alloys [7]. These properties give Nimonic 263 a wide use in marine and gas turbine engines, combustion chambers for aeronautical use, etc. [8–10].

The advantage of laser processing over conventional material processing is in the specific nature of laser light, high intensity and the possibility of controlled, precise and confined surface modification [11–13]. Since the invention of lasers, surface modifications of various metals and their alloys, performed by various types of laser irradiation, have gained considerable attention of the researchers and industry. During the interaction

between the material and the high-energy short-pulse laser, high-temperature plasma is generated and it creates shock waves on the surface of the material, which further causes plastic deformation of the material. Also, the short pulse duration of the laser can cause surface melting which leads to tensile stress. Besides laser welding, cutting, drilling and other laser-based material processing techniques, laser irradiation can be used for modification of the surface in order to improve the surface characteristics and mechanical properties of the material. Various laser surface treatments are of great importance [14], such as laser polishing [15,16] of surface hardening [17], surface cladding [18], and thermal spraying [19–21].

Mechanical and thermomechanical processing by laser irradiation has been in the focus of research interest, as a promising tool for improving these characteristics [22,23]. The basics of laser mechanical processing is the introduction of compressive residual stresses in the material's depth, by generating shock waves to achieve improvement in the microstructural and surface characteristics [24,25].

Laser shock processing can be a thermomechanical and mechanical treatment, as reported by Peyre et al. [26]. Laser mechanical treatment is used for improvement in the material's properties, especially fatigue, stress corrosion cracking, intergranular corrosion, etc. [14]. Munther et al. [27] discussed the recent progress in the laser mechanical treatment of additively manufactured (AM) parts. Sikhamov et al. [28] estimated the influence of laser mechanical treatment on the fatigue properties of AA2024-T3 specimens with a fastener hole. Although in the last few decades many investigations were devoted to laser shock processing, most of them were performed in the nanosecond laser beam regime and through a transparent layer, for generating plasma confinement, and an absorption layer for thermal protection of the surface. Since the invention of the laser, there has been constant development in terms of a shorter pulse duration, from millisecond to the femtosecond range, for example the dependence of microstructure characteristics on laser wavelength [24,25]. This paper aims to contribute to the investigation of the microstructure features introduced by picosecond thermomechanical laser treatment and to compare them to nanosecond thermomechanical laser treatment. By analyzing the available data from the experimental tests of relevant materials [11,25] and geometry [29], it can be concluded that the values obtained within the analyses presented in this paper are within the expected limits.

This investigation includes analysis of the surface condition and mechanical properties after picosecond and nanosecond laser thermomechanical treatment of the surface surrounding the holes in the Nimonic 263 sheets, and the discussion of the microstructural changes arisen by the laser treatment, throughout profilometry analysis, microhardness testing and tensile testing.

2. Materials and Methods

The reinforcement by direct laser treatment is experimentally performed on the nickel alloy Nimonic 263. Sheets of the commercial Nimonic 263 alloy are cut into a rectangular shape with the dimensions 10 mm × 200 mm × 2 mm. For statistics, a series of holes 4 mm in diameter were created by mechanical drilling, as presented in Figure 1a, under the same conditions. The drilling was done in accordance with internal laboratory procedure. Surface laser modifications of the areas surrounding the holes were done subsequently on both sides of the sheets, by pulsed picosecond and nanosecond Nd:YAG lasers (EKSPLA, Vilnius, Lithuania; Quanta System SpA, Samarate, Italy, respectively), emitting in the near-IR spectrum and in accordance with the specifications given in Table 1. The output laser beam was directed and focused on the sample surface by a reflective mirror and quartz lens system (Thorlabs, NJ, USA). The focusing distance for the picosecond laser irradiation was 157 mm, and for nanosecond laser irradiation 300 mm. The laser processing setup is shown in Figure 1b. All modifications were done in the ambience conditions of standard temperature, humidity and in the air atmosphere.

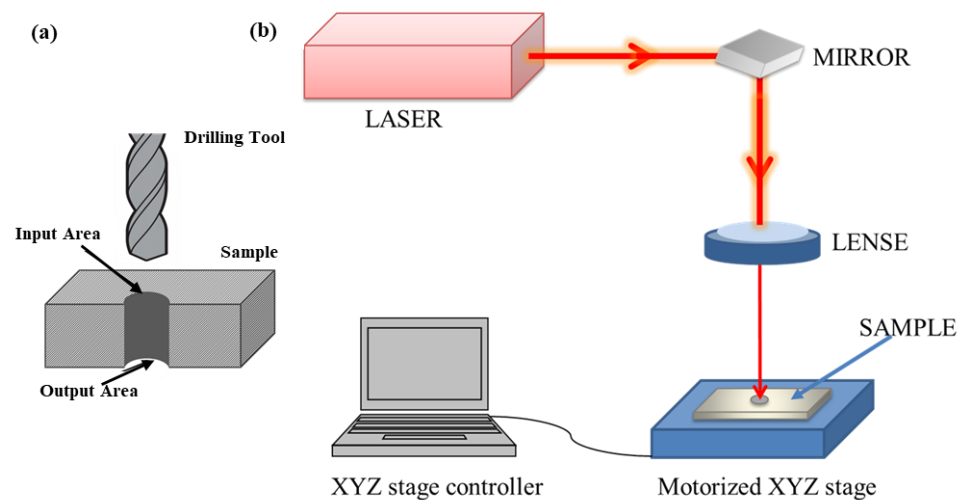


Figure 1. (a) Drilling process diagram and (b) laser processing setup.

Table 1. Specifications of picosecond and nanosecond lasers.

Lasers	Nd:YAG	Nd:YAG
Model	EKSPLA	Thunder Art-Quanta System
Wavelength	1064 nm	1064 nm
Pulse duration	170 ps	≤8 ns
Energy density	11 J/cm ²	4.24 J/cm ²
Spatial beam profile/Mode	Near TEM ₀₀	Near-field (fit to Gaussian) ≥ 0.7 Far-field (fit to Gaussian) ≥ 0.9
Repetition rate	10 Hz	20 Hz

The resulting effects were analyzed by optical microscopy (OM) (Carl Zeiss, Jena, Germany) and scanning electron microscopy (SEM) (JEOL JSM-5800, JEOL Ltd., Tokyo, Japan), and compared with the untreated surface. X-ray fluorescence XRF analysis of the Nimonic 263 alloy surface was performed with the Niton XL3t970 GOLDD+ XRF analyzer (Thermo Scientific, Waltham, MA, USA) which enables qualitative and quantitative analysis. Data processing was done with the Niton Data Transfer (NDT) software (version 6.5.5, Thermo Scientific, Waltham, MA, USA). XRF measurement average accuracy is 5%. Microhardness measurements were performed by the Vickers microhardness test using a semi-automatic model of the Hauser 249A apparatus (Muller Machines SA, Bruegg, Switzerland). Microhardness measurement accuracy is ~1.5%. The force applied was 9.807 N and the application time was 10 s. Additionally, changes in the morphologies/topography of the irradiated surfaces were analyzed using a non-contact optical profilometry (Zygo NewView 7100 Zygo Corporation, Middlefield, CT, USA), and characteristic surface parameters were calculated using MetroPro software (version 7.15.0., Zygo Corporation, Middlefield, CT, USA). The surface parameter measurement accuracy is ~5%. The modifications and measurements were done in triplicate.

Following the laser surface treatment, the effectiveness of the enhancement was analyzed by deformation and stress tests. Nimonic 263 sheets were loaded to tension with an axial force of 5 kN intensity. Deformations were determined using the ARAMIS system (version 6.1, GOM GmbH, Braunschweig, Germany) [29,30] which serves for the non-contact measurement of displacement and deformation. It is based on the digital image correlation method. The main advantage of the ARAMIS system compared to the method of strain gauges is that, in zones of significant change in stress gradient, the position of the strain gauge has a great influence on the obtained results. Using the ARAMIS system, the whole stress field could be obtained. To follow the deformation at a certain point, it is

necessary to determine the surrounding square set of pixels around that point, which is then used as a template in the pattern recognition process. The displacement resolution is in the sub-pixel range, from 0.01–0.02 pixels, and the maximum deformation accuracy is of the order size 0.02%. The measuring system was adjusted during the calibration process to ensure dimensional consistency, for correct calibration, the calibration deviation can be in the range between 0.01 and 0.04 pixels [31,32].

3. Results and Discussion

To achieve homogeneous and uniform modification of the targeted surface, and avoid extensive ablation and loss of material, the focus of the laser beam was beyond the surface. The optical images of the Nimonic 263 alloy sheets used in this experiment, before and after picosecond and nanosecond laser treatment, are presented in Figure 1. Nimonic 263 sheets are reinforced around the holes, which represent the weakest parts of the sheets, as they would be under the highest stress due to the longitudinal and transverse forces of the screw connections, and taking into consideration that the holes on the machine elements are stress concentrators.

3.1. Surface Topography Analysis

The areas around the holes on the sheets are treated with laser irradiation in order to strengthen the material around the drilled holes, in terms of reinforcing the location where the stress concentration is expected. The Nimonic 263 alloy surfaces, before and after nanosecond and picosecond laser treatment at different magnifications, are presented in Figure 2. The appearance of a hole without laser treatment is shown in Figure 2a,b. The optical image shows that two zones are distinguished at the surface outside of the hole. The inner zone, just around the hole, is spreading up to ~200 μm in width and it is the result of drilling. The outer zone is surrounding the inner zone and corresponding with the bulk surface. The area around the laser-processed hole in nanosecond mode is presented in the optical image in Figure 2d,e. Nanosecond laser processing of the material results in uniform modification, with laser spots overlapping in order to homogenize the laser beam energy distribution on the surface. The average modification of the area width around the hole is ~1.5 mm. The laser-processed area around the hole in picosecond mode is presented in the optical image in Figure 2g,h. After picosecond laser processing of the material outside the hole, the surface morphology appears uniform throughout the area affected by the laser light, with approximately 1.5 mm width around the hole. The detailed microstructure of the sheet surface before and after laser processing is also presented in Figure 2. The basic material surface is characterized by creases resulting from the surface polishing treatment as shown in Figure 2c, and the surface parameters are presented in Table 2. The nanosecond laser interaction resulted in a more even structure in the imprint itself (Figure 2f). The parallel periodic structures, average periods 260 μm , obtained by laser interaction are more pronounced with the picosecond laser (Figure 2i). The resulting surface parameters are presented in Table 2.

Besides the chemical composition, and the physical and mechanical properties, the surface topography of the parts used in the load-bearing structures plays an important role in the fatigue resistance of the structuring materials. The surface parameters of the basic material and the area surrounding the holes, prior and after nanosecond and picosecond laser treatment, are presented in Table 2. R_a represents the average surface roughness (the deviation in all points from a plane fit to a test part surface) and rms represents the root-mean-square roughness (the average of the measured height deviations taken within the evaluation area), corresponding to R_a [33]. Analyzing the values for the base material, shown in Table 2, it can be observed that the drilling process resulted in slightly increased values of the surface roughness in the area surrounding the holes, and the values of R_a and rms are increased for a factor of 1.3, as expected, due to the destructive effect of the drilling process. Following the nanosecond laser treatment, it is evident that the values of the surface roughness parameters are slightly decreased for factors of 0.8 and 0.9, for

R_a and rms , respectively. Following the picosecond laser treatment, it is evident that the values of R_a and rms are more prominently decreased, for a factor of 0.6, compared to the base material, probably due to the resolidification of the melting pool that was created during the interaction of the laser light with the base material surface. The results show that the base material is preserved as there is no crater formation or evident loss of the material due to laser ablation. These results are also confirmed by the two-dimensional surface profiles and three-dimensional surface maps of the sample before and after the laser treatment (Figure 3), which also show only changes in the surface waviness and no distinguished crater.

The SEM micrographs of the Nimonic 263 surface before the applied deformation are presented in Figure 4. Figure 4a shows the untreated surface of the Nimonic 263 alloy, with visible traces of surface polishing. After the modification by nanosecond (Figure 4b) and picosecond lasers (Figure 4c), the borders of treated and untreated areas are clearly noticeable. On the edge of the treated zones, the pores are visible, arisen after laser beam action. As the laser beam distribution is in Gauss mode, the laser energy is lower at the laser spot periphery, which results in non-uniform melting on the treated area periphery, pore creation, and parallel and radial surface structure formation. Although these pores are stress concentrators usually, in this case they were not crack initiators. According to the micrographs, these treatments were thermomechanical as there is visible melting of the material with no indication of material loss.

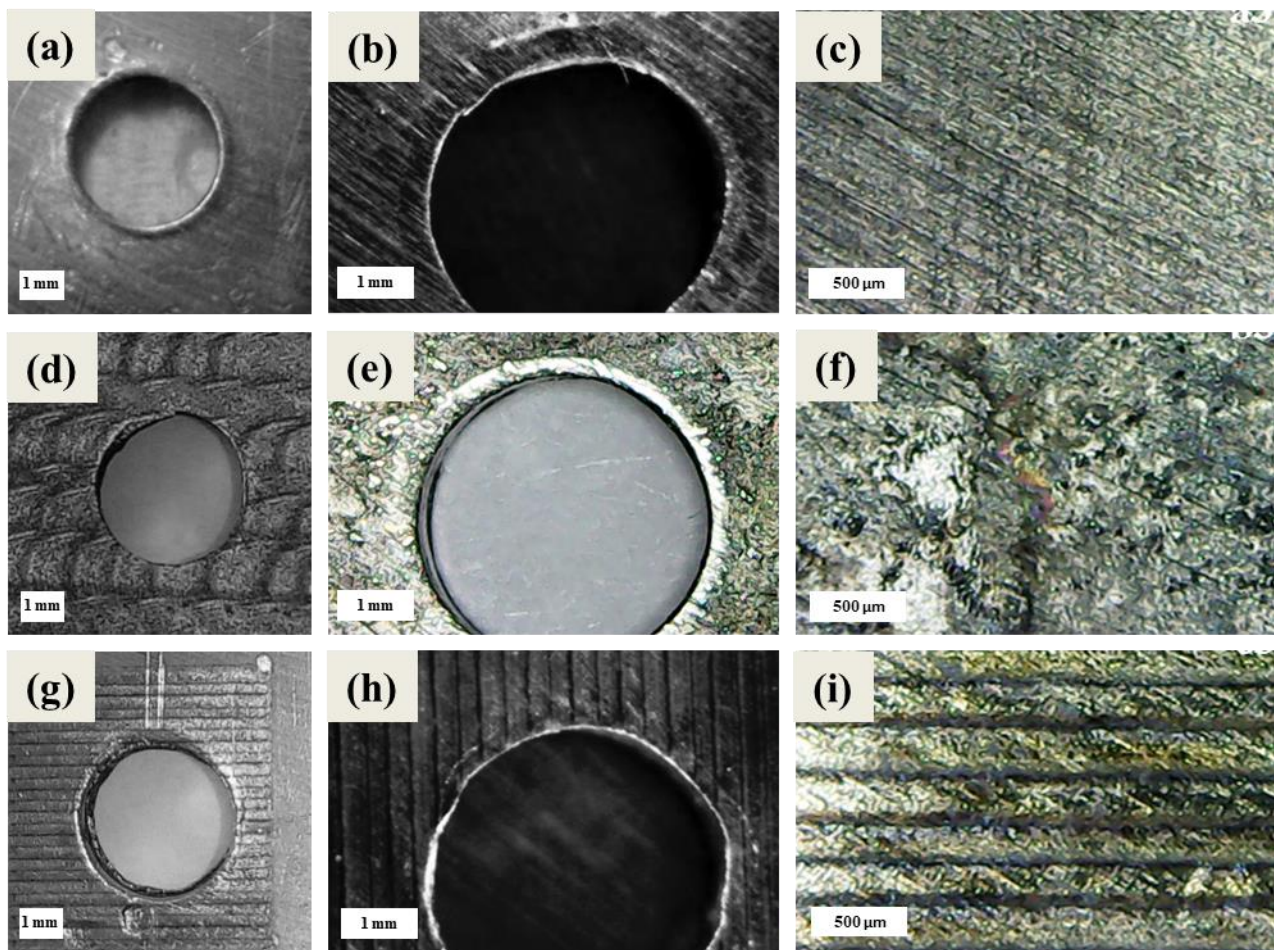


Figure 2. Microstructures around hole and surface details, as follows: larger area around the hole; area near the rim; and detail from the area near the rim: before laser treatment (a–c), after nanosecond laser treatment (d–f), and after picosecond laser treatment (g–i).

Table 2. Surface characteristics of the basic material (BM) and areas around the holes treated with picosecond laser and nanosecond laser irradiation.

Surface Parameters	Before Drilling	Zone Surrounding the Hole after Drilling	ns Laser Action	ps Laser Action
R_a [μm]	0.41 ± 0.01	0.56 ± 0.02	0.46 ± 0.01	0.33 ± 0.01
rms [μm]	0.54 ± 0.02	0.71 ± 0.03	0.64 ± 0.03	0.42 ± 0.01

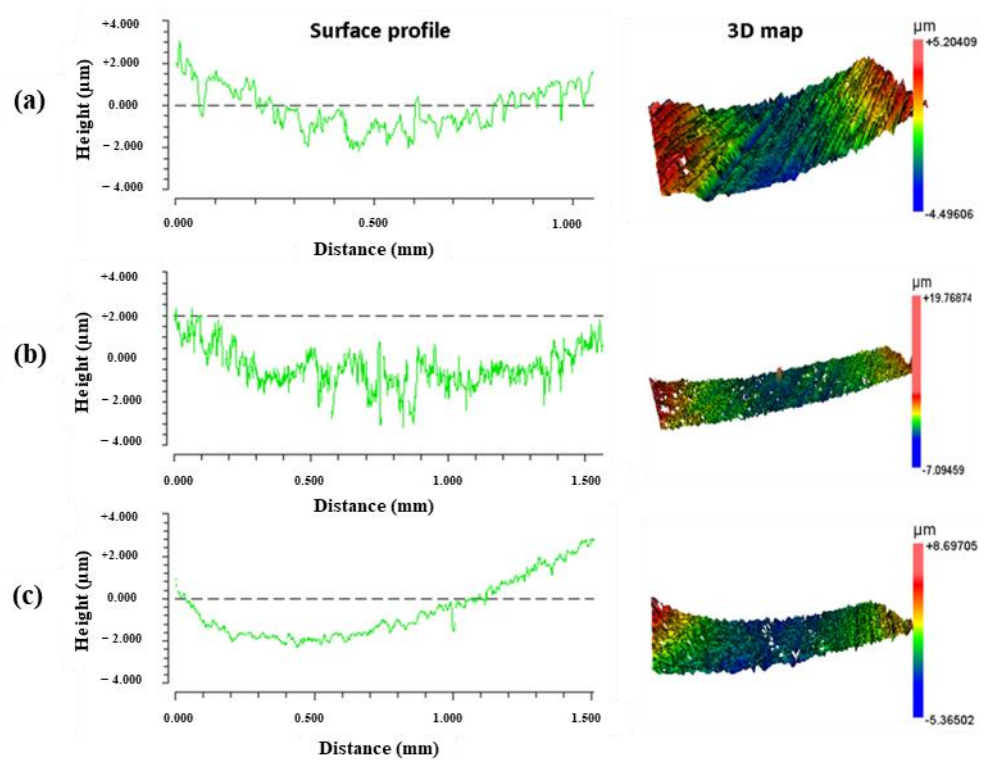


Figure 3. 2D surface profile and 3D map around the untreated hole (a) reinforced by nanosecond (b) and picosecond laser (c) treatment.

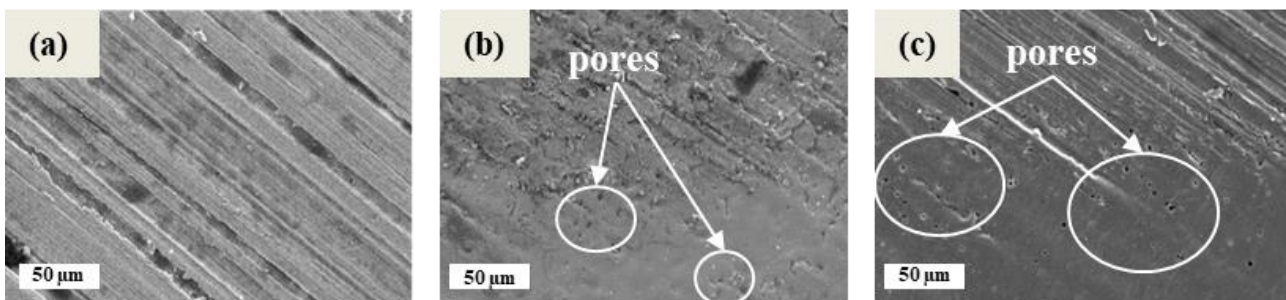


Figure 4. Scanning electron microscopy (SEM) micrographs of Nimonic 263 sample surface before laser treatment (a), and the border of the modified surface area and untreated surface area after nanosecond (b) and picosecond (c) laser treatment.

3.2. Qualitative and Quantitative Analysis

The results of the XRF analysis of Nimonic 263 before and after laser modification are presented in Table 3. Comparing the results, it can be concluded that the treatment with laser beams at both pulse durations showed no distinguished impact on the chemical composition of the Nimonic 263 superalloy. The values of the concentrations of the elements present in the sample match well with the untreated and laser-treated sample, within the limits of the instrument measurement error (2σ). These results are in agreement with the overall goal of this investigation which is the non-destructive modification of the surface of interest and the preservation of the surface chemical composition.

Table 3. Results of the X-ray fluorescence XRF qualitative and quantitative analysis.

Elemental Composition	Untreated Sample	Nanosecond Laser Treatment	Picosecond Laser Treatment
Element	Concentration (%)	Concentration (%)	Concentration (%)
Mo	5.92 ± 0.03	5.97 ± 0.03	5.91 ± 0.04
Si	0.30 ± 0.02	0.31 ± 0.05	0.36 ± 0.04
Ni	52.41 ± 0.11	52.44 ± 0.15	52.23 ± 0.19
Co	20.06 ± 0.10	20.16 ± 0.11	20.06 ± 0.13
Fe	0.69 ± 0.02	0.69 ± 0.03	0.63 ± 0.03
Mn	0.35 ± 0.04	0.35 ± 0.04	0.47 ± 0.05
Cr	18.76 ± 0.08	18.41 ± 0.09	18.55 ± 0.10
Ti	1.76 ± 0.05	1.62 ± 0.05	1.69 ± 0.05

3.3. Testing of Mechanical Properties

The microhardness values measured by the Vickers test are presented on the diagram in Figure 5. The values obtained represent the mean of the microhardness measured around all the holes. The results show that the applied laser modification increases the microhardness value of the Nimonic base material by ~10 percent and 14.5 percent, after nanosecond and picosecond laser processing, respectively, thus achieving the proposed enhancement of the base material.

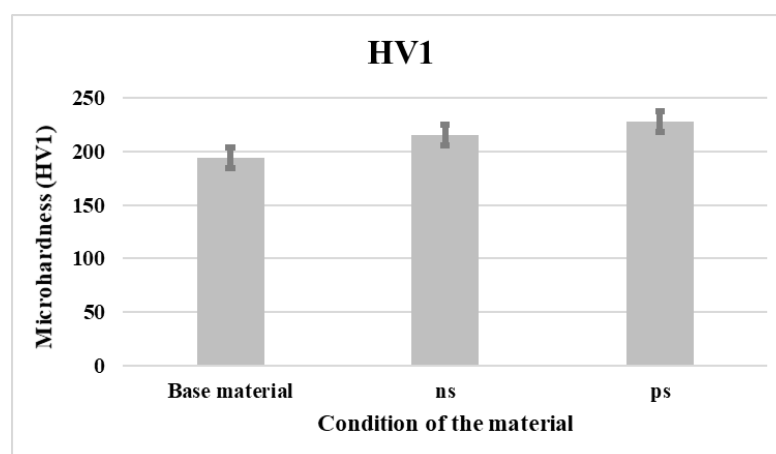


Figure 5. Diagram of microhardness values depending on material condition before deformation and after ns and ps laser treatment.

Various processes that occur during the laser interaction with the metallic/alloy surface have an impact on the thermal, mechanical, electric and optical characteristics of the treated materials, as well as their surface and subsurface structure. Laser surface treatment is based on generating high-pressure shock waves on the target surface, if using a high-intensity laser beam [34]. The value of the generated compressive residual stresses is maximal on the surface and decreases into the depth of the material [14]. Shock waves

can cause the following two distinguished effects: microstructure alterations on the surface and below the impact surface, and the generation of high-density dislocations [35]. The combination of these effects contributes to the enhancement of the mechanical properties near the affected material surface.

As noted above, deformations are measured using the digital image correlation (DIC) method, and the GOM optical system and ARAMIS software are used to perform 3D experimental optical analysis of the specimens [29,30].

After calibration of the system and specimen is successfully performed, as shown in Figure 6, the experimental measurement procedure was performed, i.e., the measuring project was created in the software and during various loading stages of the object, and the images were recorded. During the test, the forces and the displacement were recorded.

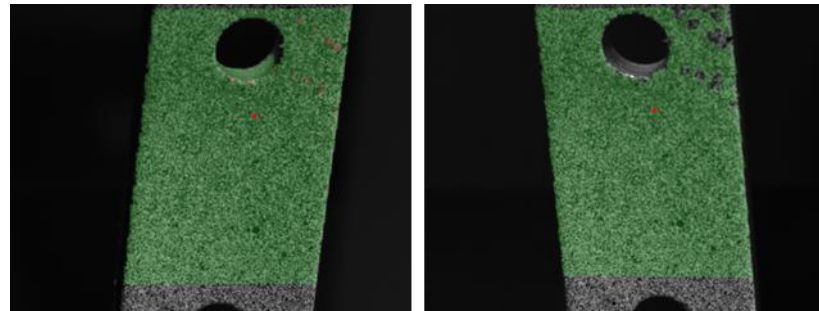


Figure 6. Recorded field, left and right camera.

Figures 7–9 show reports for the initial stage, i.e., undeformed state, and the final stage, i.e., deformed state due to a given load for the untreated Nimonic 263 sample, Nimonic 263 treated by nanosecond laser irradiation and Nimonic 263 treated by picosecond laser irradiation, respectively. All the specimens are loaded to tension with an axial force of 5 kN intensity.

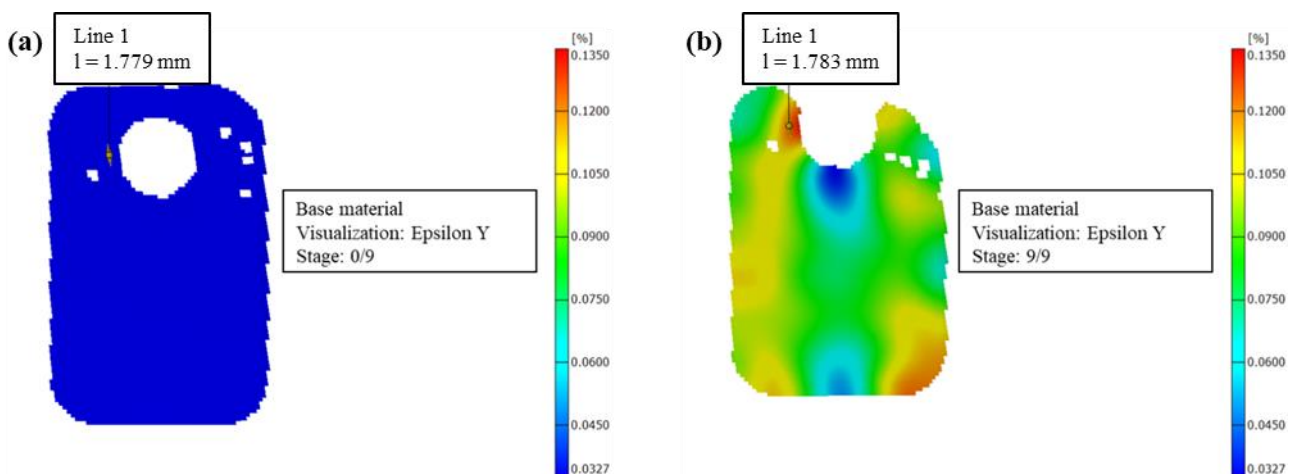


Figure 7. Nimonic 263 sheet, base material digital image correlation (DIC) measurement 1: (a) unloaded state, and (b) axial force 5 kN.

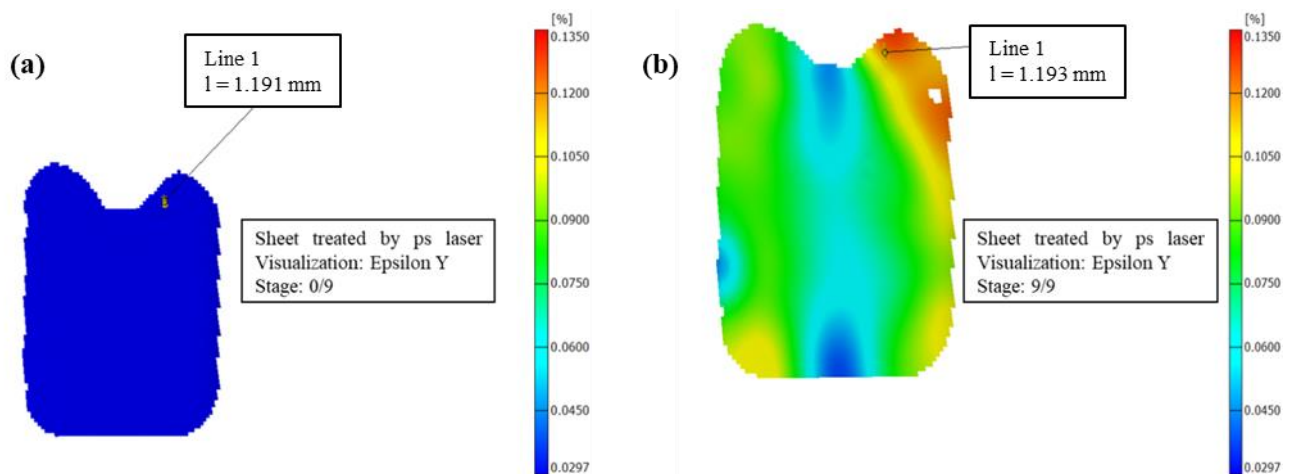


Figure 8. Nimonic 263 sheet, treated by ps laser DIC measurement 1: (a) unloaded state, and (b) axial force 5 kN.

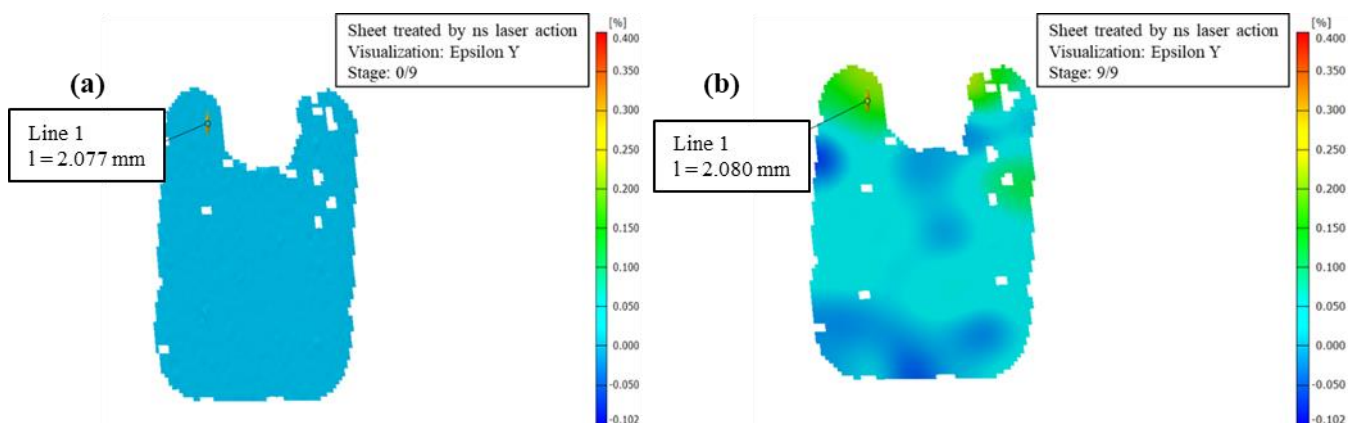


Figure 9. Nimonic 263 sheet, treated by ns laser action DIC measurement 1: (a) unloaded state, and (b) axial force 5 kN.

During the measurement, the method of linear deformation was applied, when the deformation is determined between the central measuring point, by establishing its relationship to the surrounding measuring points. In accordance with the theory of axially loaded rods, the deformation field is in line with the expectations, i.e., stress concentrations occur due to the existence of openings and the reduction in the cross-section [29]. The results of this study show the strain field with the longitudinal load acting upon the specimen, and the results are given in the form of field images of the specimens in the unloaded state and the final loaded state. All the images show one line in the stress concentration zone, which simulates a strain gauge. By comparing the length of the line in the undeformed and deformed state, the value of deformation, ε (BM in the index denotes base material, PLM denotes picosecond laser-reinforced material, NLM denotes nanosecond laser-reinforced material), is obtained, and by recalculation, based on Hooke's law, the value of stress, σ (BM in the index denotes base material, PLM denotes picosecond laser-reinforced material, NLM denotes nanosecond laser-reinforced material), is obtained. The line is placed parallel to the axis of the specimen since the tile is loaded in the longitudinal direction. Likewise, the deformation fields shown refer to the longitudinal direction, so ε is shown, not the equivalent von Mises deformation.

The appearance of the deformation field is in line with the expectations, the stress concentration zone (and deformation zone) is located laterally from the hole, where the cross-section is weakened.

From the DIC measurements for the Nimonic 263 sheet, base material, it can be assumed that plastic deformation of the zone of highest stresses due to the maximal

loading has occurred, and it can be seen from the diagrams shown that the zone of highest stresses is not lateral to the hole but at an angle (Figure 7). The calculated result for the maximum average value of deformation, ϵ_{BM} , obtained using the reference points in a loaded and unloaded state, is 0.00225 ± 0.00001 . The calculated result for the maximum average value of stress, σ_{BM} , obtained by Hooke's law, is (503.6 ± 0.1) MPa. The Young's modulus of elasticity for Nimonic 263 was found to be 22.4×10^4 MPa, the yield stress for Nimonic 263 was found to be 585.0 MPa, and the tensile strength value is 1004 MPa [36]. Considering the calculated stress in the stress concentration zone (503.6 MPa), it can be seen that the yield stress has not been reached.

From the DIC measurements of the picosecond laser-treated Nimonic 263 sheet, it is noticed that the stress concentration zone is not lateral to the hole, which is to be expected considering that the zone lateral to the hole is laser-reinforced (Figure 8). The calculated result for the maximum average value of deformation, ϵ_{PLM} , obtained using the reference points in a loaded and unloaded state, is 0.00168 ± 0.00001 . The calculated result for the maximum average values of stress, σ_{PLM} , obtained by Hooke's law, is (376.2 ± 0.1) MPa.

From the diagrams shown and the DIC measurements for the nanosecond laser-treated Nimonic 263 sheet, it can be seen that the stress concentration zone is not lateral to the hole (Figure 9). The calculated result for the maximum average value of deformation, ϵ_{NLM} , obtained using the reference points in a loaded and unloaded state, is 0.00144 ± 0.00001 . The calculated result for the maximum average value of stress, σ_{NLM} , obtained by Hooke's law, is (323.1 ± 0.1) MPa.

It is evident that the laser modification of the surface surrounding the hole is causing the improvement in resilience to deformation, since the deformation value of the base material, is decreased by ~27 percent and ~40 percent, for picosecond and nanosecond laser action, respectively. The value of stress is also decreased by ~25 percent and ~36 percent, for picosecond and nanosecond laser action, respectively. These results have shown that nanosecond laser treatment gave the lowest values of deformation and stress, which indicates that the best mechanical characteristics are achieved by such reinforcement of the material.

The inner surface of the untreated material is presented in Figures 10a and 11c,d, and it can be noted that the damages are arisen by both the drill and tensile test. Although, the inner surfaces of the holes treated by picosecond laser irradiation (Figures 10b and 12c,d) and nanosecond laser irradiation (Figures 10c and 12g,h), were not directly exposed to laser beams, those surfaces are obviously affected and rather less damaged after tensile tests than the surface of untreated material. The cracks arisen after the tensile test on the picosecond laser-treated material are observable by visual inspection (Figure 10b), while the microcracks arisen after the tensile test on the nanosecond laser-treated material are not visible (Figure 10c). Microcracks are observed by SEM (Figures 11 and 12), and it can be noticed that these non-favourable phenomena more frequently appear in the cross sections compared to the outer surface, because the inner part of the hole was also exposed to the laser irradiation, but the incidence angle of the laser beam was below 90 degrees.

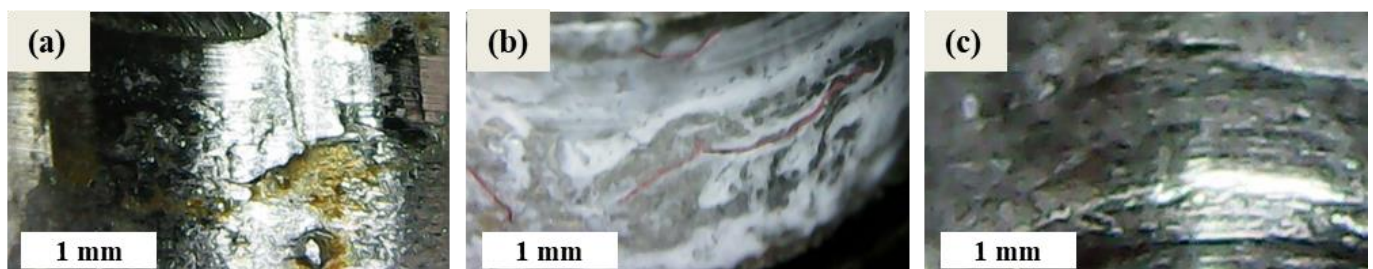


Figure 10. Inner hole surfaces of (a) untreated (b) picosecond laser-treated (c) nanosecond laser-treated material.

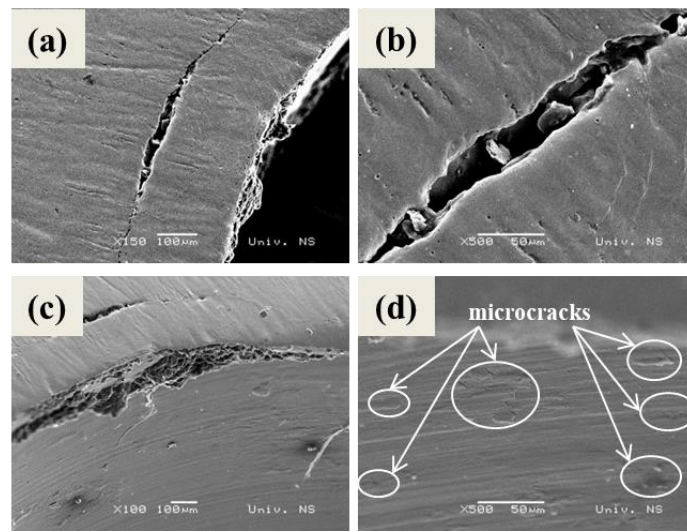


Figure 11. Micrographs after tensile test of untreated material (a–d).

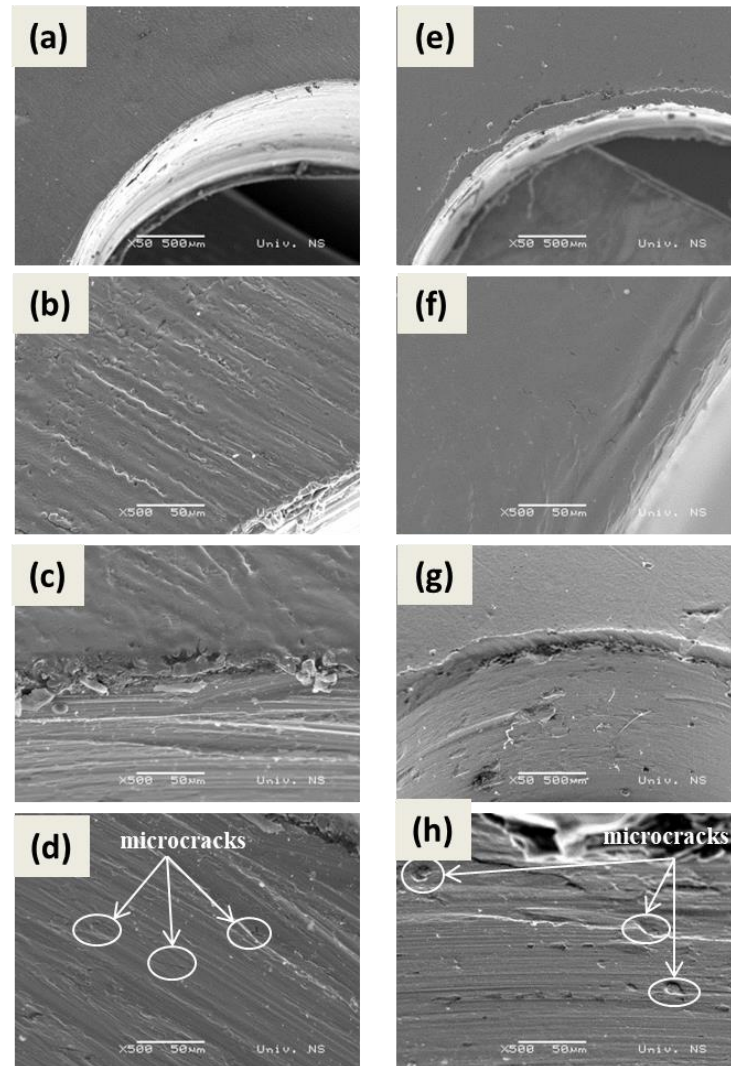


Figure 12. Micrographs after tensile test of the following: (a–d) material surface treated by nanosecond laser irradiation and (e–h) material surface treated by picosecond laser irradiation.

The SEM micrographs (Figures 11 and 12) confirm the results obtained by the tensile tests. The micrographs in Figure 11a,b are taken at the outer surface of the untreated sample after the tensile tests, at the rim of the hole, at different magnifications. Figure 11a,b presents the microcrack arisen after the tensile test. Although the tensile test caused the microcrack formation, there is a high probability that the unwanted phases, visible in the microcrack, helped its formation and propagation. The micrographs in Figure 12a,b are taken at the outer surface of the sample, treated by nanosecond laser irradiation, at the rim of the hole, at different magnifications, and the micrographs from Figure 12c,d are taken at the inner wall of the hole, at different magnifications. The micrographs in Figure 12e,f are taken at the outer surface of the sample, treated by picosecond laser irradiation, at the rim of the hole, at different magnifications, and the micrographs from Figure 12g,h are taken at the inner wall of the hole, at different magnifications. The cracks on the surface around the hole on the untreated material are significantly longer (up to 800 μm long) (Figure 11a,b) compared to the cracks propagated on the surface of the picosecond-treated material (up to 200 μm) (Figure 12e,f), while after nanosecond treatment the microcracks are not longer than 8 μm (Figure 12a,b). Also, the width of the cracks are up to 20 μm after the tensile test of untreated material, 20 times wider than after the tensile tests of the picosecond or nanosecond laser-treated material. The number of microcracks arisen in the deformed untreated material is significantly higher than in the material laser treated before deformation. The inner area of the untreated hole is visibly rougher and more uneven than the inner area of the holes treated by nanosecond and picosecond laser irradiation. The rims of the treated holes are smoother and without unwanted excess material, resulting in the more reliable construction. Following the deformation and stress tests, and SEM investigation, observed microcracks more frequently appear in the cross sections.

4. Conclusions

The presented study showed the results and effects of the laser processing of the Ni-based superalloy Nimonic 263 surface area, susceptible to stress concentration. Surface laser modifications of the areas surrounding the holes drilled in Nimonic 263 sheets are done by pulsed picosecond and nanosecond Nd:YAG laser irradiations. The areas around holes are treated with laser irradiation in order to reinforce the material around the drilled holes, in terms of reinforcing the location where the stress concentration is expected. The following can be concluded:

- 1 Following the nanosecond laser treatment, the values of the surface roughness parameters are slightly decreased for factors of 0.8 and 0.9, for R_a and rms , respectively. Following the picosecond laser treatment, it is evident that the values of R_a and rms are more prominently decreased, for a factor of 0.6, compared to the base material. The results show that the base material is preserved as there is no crater formation or evident loss of the material due to laser ablation;
- 2 Surface treatment with laser beams at both pulse durations showed no distinguished impact on the chemical composition of the Nimonic 263 superalloy. The values of the concentrations of the elements present in the sample match well for the untreated and laser-treated sample, and show that applied laser processing is non-destructive, with preservation of the surface chemical composition;
- 3 The results of the microhardness tests show that the applied laser modification increases the microhardness value of the Nimonic base material by ~10 percent and 14.5 percent, after nanosecond and picosecond laser processing, respectively, thus achieving the proposed enhancement of the base material;
- 4 Laser modification of the surface surrounding the hole is causing the improvement in the resilience to deformation, since the deformation value of the base material is decreased by ~27 percent and ~40 percent, for picosecond and nanosecond laser action, respectively. The value of stress is also decreased by ~25 percent and ~36 percent, for picosecond and nanosecond laser action, respectively;

- 5 Following the deformation and stress tests, observed microcracks more frequently appear in the cross sections compared to the outer surface which was reinforced by direct laser action. The dimensions of the cracks on the surface around the hole on the untreated material are significantly larger compared to the cracks propagated on the surface treated by the picosecond and nanosecond laser irradiation.

Author Contributions: Conceptualization, S.P.; formal analysis, B.R.; investigation, B.R., K.Č., A.P., Ž.M. and D.M.; methodology, S.P.; resources, S.P.; software, B.R., K.Č., A.P., Ž.M. and D.M.; supervision, D.M.; writing—original draft, B.R., S.P. and D.M.; writing—review and editing, Z.S. All authors have read and agreed to the published version of the manuscript.

Funding: This research was financially supported by the Ministry of Education, Science and Technological Development of the Republic of Serbia, under contract numbers 451-03-9/2021-14/200051, 451-03-9/2021-14/200131 and 451-03-9/2021-14/200105, and the Central Institute for Conservation, Belgrade, Serbia.

Data Availability Statement: Not applicable.

Conflicts of Interest: The authors declare no conflict of interest.

References

1. Reed, R.C. *The Superalloys: Fundamentals and Applications*; Cambridge University Press: London, UK, 2006.
2. Lee, H.T.; Hou, W.H. Development of fine-grained structure and the mechanical properties of nickel-based Superalloy 718. *Mater. Sci. Eng. A* **2012**, *555*, 13–20. [[CrossRef](#)]
3. Pollock, T.M.; Tin, S. Nickel-Based Superalloys for Advanced Turbine Engines: Chemistry, Microstructure, and Properties. *J. Propuls. Power* **2006**, *22*, 361–374. [[CrossRef](#)]
4. Shahriari, D.; Sadeghi, M.H.; Akbarzadeh, A.; Cheraghzadeh, M. The influence of heat treatment and hot deformation conditions on γ' precipitate dissolution of Nimonic 115 superalloy. *Int. J. Adv. Manuf. Technol.* **2009**, *45*, 841–850. [[CrossRef](#)]
5. Singh, P.N.; Singh, V. Influence of ageing treatment on work hardening behaviour of a Ni-base superalloy. *Scr. Mater.* **1996**, *34*, 1861–1865. [[CrossRef](#)]
6. Park, N.K.; Kim, I.S.; Na, Y.S.; Yeom, J.T. Hot forging of a nickel-base superalloy. *J. Mater. Process. Technol.* **2001**, *111*, 98–102. [[CrossRef](#)]
7. Sharma, A.K.; Anand, M.; Kumar, V.; Kumar, S.; Das, A.K. Laser Beam Treatment of Nimonic C263 Alloy: Study of Mechanical and Metallurgic Properties. In *Advances in Micro and Nano Manufacturing and Surface Engineering*; Shunmugam, M.S., Kanthababu, M., Eds.; Springer: Singapore, 2019; pp. 633–646.
8. Li, Q.; Yang, L.; Hou, C.; Adeyemi, O.; Chen, C.; Wang, Y. Surface ablation properties and morphology evolution of K24 nickel based superalloy with femtosecond laser percussion drilling. *Opt. Lasers Eng.* **2019**, *114*, 22–30. [[CrossRef](#)]
9. Romero-Jabalquinto, A.; Velasco-Tellez, A.; Zambrano-Robledo, P.; Bermudez-Reyes, B. Feasibility of manufacturing combustion chambers for aeronautical use in Mexico. *J. Appl. Res. Technol.* **2016**, *14*, 167–172. [[CrossRef](#)]
10. Zhao, J.C.; Ravikumar, V.; Beltran, A.M. Phase Precipitation and Phase Stability in Nimonic 263. *Metall. Mater. Trans. A* **2001**, *32*, 1271–1282. [[CrossRef](#)]
11. Petronić, S.; Čolić, K.; Đorđević, B.; Milovanović, D.; Burzić, M.; Vučetić, F. Effect of laser shock peening with and without protective coating on the microstructure and mechanical properties of Ti-alloy. *Opt. Lasers Eng.* **2020**, *129*, 106052. [[CrossRef](#)]
12. Wang, H.; Jurgensen, J.; Decker, P.; Hu, Z.; Yan, K.; Gurevich, E.L.; Ostendorf, A. Corrosion behavior of NiTi alloy subjected to femtosecond laser shock peening without protective coating in air environment. *Appl. Surf. Sci.* **2020**, *501*, 144338. [[CrossRef](#)]
13. Salimianrizi, A.; Foroozmehr, E.; Badrossamay, M.; Farrokhpour, H. Effect on Laser Shock Peening on surface properties and residual stress of Al6061-T6. *Opt. Lasers Eng.* **2016**, *77*, 112–117. [[CrossRef](#)]
14. Sundar, R.; Ganesh, P.; Gupta, R.K.; Ragvendra, G.; Pant, B.K.; Vivekanand, K.; Ranganathan, K.; Rakesh, K.; Bindra, K.S. Laser Shock Peening and its Applications: A Review. *Lasers Manuf. Mater. Process.* **2019**, *6*, 424–463. [[CrossRef](#)]
15. Marimuthu, S.; Triantaphyllou, A.; Antar, M.; Wimpenny, D.; Morton, H.; Beard, M. Laser polishing of selective laser melted components. *Int. J. Mach. Tools Manuf.* **2015**, *95*, 97–104. [[CrossRef](#)]
16. Temmler, A.; Liu, D.; Preußner, J.; Oeser, S.; Luo, J.; Poprawe, R.; Schleifenbaum, J.H. Influence of laser polishing on surface roughness and microstructural properties of the remelted surface boundary layer of tool steel H11. *Mater. Des.* **2020**, *192*, 108689. [[CrossRef](#)]
17. Moradi, M.; Sharif, S.; Nasab, S.J.; Moghadam, M.K. Laser surface hardening of AISI 420 steel: Parametric evaluation, statistical modeling and optimization. *Optik* **2020**, *224*, 165666. [[CrossRef](#)]
18. Siddiqui, A.A.; Dubey, A.K. Recent trends in laser cladding and surface alloying. *Opt. Laser Technol.* **2021**, *134*, 106619. [[CrossRef](#)]
19. Wen, Z.; Dejun, K. Effects of laser thermal sprayed AlNiCr coating on fatigue performances of S355 structural steel. *Int. J. Fatigue* **2020**, *131*, 105359. [[CrossRef](#)]

20. Wu, H.; Kong, D. Effects of laser power on friction-wear performances of laser thermal sprayed Cr₃C₂-NiCr composite coatings at elevated temperatures. *Opt. Laser Technol.* **2019**, *117*, 227–238. [[CrossRef](#)]
21. Zhao, W.; Kong, D. Effects of laser power on immersion corrosion and electrochemical corrosion performances of laser thermal sprayed amorphous AlFeSi coatings. *Appl. Surf. Sci.* **2019**, *481*, 161–173. [[CrossRef](#)]
22. Thomas, M.; Jackson, M. The role of temperature and alloy chemistry on subsurface deformation mechanisms during shot peening of titanium alloys. *Scr. Mater.* **2012**, *66*, 1065–1068. [[CrossRef](#)]
23. Li, K.; Fu, X.S.; Chen, G.Q.; Zhou, W.L.; Li, Z.Q. Mechanical properties of strengthened surface layer in Ti-6Al-4V alloy induced by wet peening treatment. *Trans. Nonferrous Met. Soc. China* **2016**, *26*, 2868–2873. [[CrossRef](#)]
24. Shepard, M.J.; Smith, P.R.; Amer, M.S. Introduction of compressive residual stresses in Ti-6Al-4V simulated airfoils via laser shock processing. *J. Mater. Eng. Perform.* **2001**, *10*, 670–678. [[CrossRef](#)]
25. Petrovic, S.; Sibalija, T.; Burzic, M.; Polic, S.; Colic, K.; Milovanovic, D. Picosecond Laser Shock Peening of Nimonic 263 at 1064 nm and 532 nm Wavelength. *Metals* **2016**, *16*, 41. [[CrossRef](#)]
26. Peyre, P.; Chaieb, I.; Braham, C. FEM calculation of residual stresses induced by laser shock processing in stainless steels. *Model. Simul. Mat. Sci. Eng.* **2007**, *15*, 205–221. [[CrossRef](#)]
27. Munther, M.; Martin, T.; Tajyar, A.; Hackel, L.; Beheshti, A.; Davami, K. Laser shock peening and its effects on microstructure and properties of additively manufactured metal alloys: A review. *Eng. Res. Express* **2020**, *2*, 022001. [[CrossRef](#)]
28. Sikhamov, R.; Fomin, F.; Klusemann, B.; Kashaev, N. The Influence of Laser Shock Peening on Fatigue Properties of AA2024-T3 Alloy with a Fastener Hole. *Metals* **2020**, *10*, 495. [[CrossRef](#)]
29. Tatić, T.; Čolić, K.; Sedmak, A.; Mišković, Ž.; Petrović, A. Evaluation of the Locking Compression Plates Stress-Strain Fields. *Techn. Gazette* **2018**, *25*, 112–117. [[CrossRef](#)]
30. Čolić, K.; Gubeljak, N.; Burzić, M.; Sedmak, A.; Mijatović, T.; Milovanović, A. Analysis of fracture behaviour of thin s316l stainless steel plates. *Struct. Integr. Life* **2017**, *17*, 211–216, UDC: 620.172.24:669.14.018.8.
31. ARAMIS. Hardware, aramis_hw_en_rev-c, Braunschweig, Germany, 2007, User Information.
32. ARAMIS. Software, aramis_v6_1st_en_rev-c, 2007, User Manual.
33. MetroPro Surface Texture Parameters. Available online: https://www.lambdaphoto.co.uk/pdfs/Surface_Texture.pdf (accessed on 12 November 2020).
34. Peyre, P.; Fabbro, R. Laser shock processing: A review of the physics and applications. *Opt. Quantum Electron.* **1995**, *27*, 1213–1229. [[CrossRef](#)]
35. Peyre, P.; Scherpereel, X.; Berthe, L.; Carboni, C.; Fabbro, R.; Beranger, G.; Lemaitre, C. Surface modifications induced in 316L steel by laser peening and shot-peening. Influence on pitting corrosion resistance. *Mater. Sci. Eng. A* **2000**, *280*, 294–302. [[CrossRef](#)]
36. Aircraft Materials. Available online: <https://www.aircraftmaterials.com/data/nickel/C263.html> (accessed on 17 April 2021).